Zeroth-order finite similitude and scaling of complex geometries in biomechanical experimentation

Raul Ochoa-Cabrero [1] Teresa Alonso-Rasgado [3] Keith Davey[2]

affiliations: [1] Department of Materials Science, The University of Manchester, Manchester, UK

[2] Department of Mechanical, Aerospace and Civil Engineering, The University of Manchester, Manchester, UK

[3] Queen Mary University of London, London, UK

abbreviated title: Zeroth-Order Similitude in Biomechanics

correspondence: Keith Davey, School of Mechanical, Aerospace and Civil Engineering, The University of Manchester, Manchester, UK

Tel.: +44 (0) 161 306 3834

e-mail: keith.davey@manchester.ac.uk

Abstract

Scaled experimentation provides an alternative approach to full-scale biomechanical (and biological) testing but is known to suffer from scale effects, where the underlying system behaviour changes with scale. This phenomenon is arguably the overriding principal obstacle to the many advantages that scaled experimentation provides. These include reduced costs, materials and time, along with the eschewal of ethical compliance concerns with the application of substitute artificial materials as opposed to the use of hazardous biological agents.

This paper examines the role scale effects play in biomechanical experimentation involving strain measurement and introduces a formulation that overtly captures scale dependencies arising from geometrical change. The basic idea underpinning the new scaling approach is the concept of space scaling, where a biomechanical experiment is scaled by the metaphysical mechanism of space contraction.

The scaling approach is verified and validated with finite element models and actual physical-trial experimentation using digital image correlation software applied to synthetic composite bone. The experimental design aspect of the approach allows for the selection of 3D printing materials for trial-space analysis in a complex pelvis geometry. This aspect takes advantage of recent advancements in additive manufacturing technologies with the objective of countering behavioural distorting scale effects.

Analysis is carried out using a laser confocal microscope to compare the trial and physical space materials and subsequently measured using surface roughness parameters. Finite element models were constructed for the left hemipelvis and results show similar strain patterns (average percentage error $< 10\%$) for two of the three trial-space material combinations. A Bland Altman statistical analysis shows a good agreement between the finite element models and physical experimentation and a good agreement between the physical-trial experimentation providing good supporting evidence of the applicability of the new scaling approach in a wider range of experiments.

keywords: Scaling, Biomechanical, Similitude, Trial experimentation

1 Introduction

Scaled experimentation has many advantages and principal among them is the significant reduction in cost associated with scaling, which has invariably led to its application in a plethora of subject areas[1,2,3]. In the case of biological research and specifically biomechanical experimentation the more common testing includes cadaveric studies or cultivated tissue where many obstacles arise when dealing with the extensive testing of biological materials: ethical compliance issues, availability of resources and sample preparation can hinder research considerably[4,5]; *in vivo* studies suffer even more from these problems. The collection and preservation of specimens is a major factor in these studies[4] and thus variability between them poses concerns (wet and dry bone have substantially different material properties), there is also variation with age and cadaveric specimens are biased to the elder part of the population[5]. A good solution to the variability issue is the use of synthetic composite bone which has been proven useful and can be considered a standard for the mechanical properties and geometry of bone[5].

Another important concern when dealing with biological systems is the fact that in practice it is often difficult to obtain measurements without affecting the biological system itself, which often comes at the cost of accuracy using indirect methods of measurement[6]. The use of finite element (FE) modelling has been particularly useful in this regard; the complex geometries and ethical concerns can be solved using finite element analysis in muscular skeletal systems. These are used to study a variety of subjects from the optimization of the position of the acetabulum in a periacetabular osteotomy[7] to the analysis of the bone-cement interface for different prosthetic femoral head sizes after total hip arthroplasty[8]. They have become increasingly popular in recent years since they allow for the optimisation of medical procedures or testing of biomedical materials without the associated risk for the patient and have seen much improvement[5]. Models have to be validated in order to ensure the reliability of any results obtained; the use of digital image correlation (DIC) software and synthetic composite bone have been shown to replicate the results obtained from strain rosette measurements and cadaveric bone thus providing a good methodology for their validation[9].

The cost of experimentation however remains high and the availability of materials can be an obstacle; the design of scaled experimentation that solves these issues is of great interest in the field of biomechanical research. The most common scaling approach is dimensional analysis[10,11], which is based on the notion that physics does not depend on the choice of units and the central theorem (Buckingham Pi) provides a means to obtain dimensionless parameters or Pi groups that reduce the necessary parameters used to describe the physics of the phenomena. The approach achieves any form of scaling indirectly by assuming the governing equations remain invariant for both scales and using these Pi groups to relate properties at the full and trial-scales. In experimental reality, scale invariance is seldom the case, and its success therefore is often reliant on expertise in the selection of governing parameters or full-scale experimentation is unavoidable. This invariably leads to increases in the cost of the research and if it transpires that the matching of parameters cannot be achieved, then the approach offers no solution since there is no element of experimental design.

An alternative scaling approach that has recently been developed has proven successful to a certain extent in the field of biomechanical experimentation[12,13]; the concept of finite similitude. The fundamental idea of finite similitude is the fact that the physics in general cannot be guaranteed to scale but conservation (and some non-conservative) laws must hold over an extensive range of scales (where continuum mechanics is valid). The scaling approach uses the construction of a scaling map ($\mathbf{x}_1 \mapsto \mathbf{x}_\beta$), that relates coordinate functions of inertial frames in the physical and trial spaces, and indirectly characterises the deformation of space using the notion of deformation from a continuum perspective. The scaling map facilitates the relating of transport equations in both spaces and consequently provides the means to assess the effects of scaling. For biomechanical experimentation consisting of validation of finite element models by means of digital image correlation and synthetic composite bone the conservation laws for volume, mass and momentum apply along with the non-conservation law for movement, which brings displacement (see reference[14]) into the family of transport forms. All these equations have to be satisfied and related in order to guarantee that the

governing physics remains representative in both the physical and trial spaces.

The projection of trial space onto the physical space (i.e. via the map $\mathbf{x}_1 \mapsto \mathbf{x}_\beta$) to produce a virtual model is a critical feature as it reveals both explicit and implicit changes caused by scale in the transport equations. The changes in volume and area are explicit whilst other changes although captured in the transport equations are hidden. The exposure of implicit scale dependencies is achieved by the application of a scale-invariant identity, which in this paper is restricted to the first derivative only. Integration of the identity reveals proportionality in the physical fields and a set of scaling parameters whose purpose is the annihilation of the length-scale parameter. The element of experimental design particular to the approach arises from the consideration of the constitutive response that allows for the selection of material properties in the trial space. These can then be compared to the virtual trial-space material properties (using a projection of the physical-space model) to assess the success of the approach; it is possible also to use scaling to compare properties in the physical space (using a projection of the trial-space model). The approach leaves the relationships for scaling between spaces clearly stated, while exact similitude is seldom achieved since the virtual material properties might not be properties that any existing material may possess, the quantification of the mismatch and experimental design can assist the improvement of any proposed trial experimentation.

The statement and application of the zeroth-order finite similitude approach in the field of biomechanical experimentation is presented in Section 2, the fundamental notions of the approach that consists in characterising the distortion of space are introduced using the balance laws in transport form to obtain the similarity equations that are fundamental for the novel scaling approach. A set of scaling parameters are introduced to provide greater flexibility when selecting material properties and thus assisting the design of trial experimentation. Following the methodology the balance laws of volume, continuity, momentum and movement (Sections 2.2, 2.3, 2.4 and 2.5) impose constraints that eventually, using the constitutive response, leads to the selection of trial-space materials presented in Section 2.8 that solve the main issues that arise when considering biomechanical experimentation

used when validating finite element models by means of image correlation software and synthetic composite bone. Advancements in additive manufacturing technology allows for the improvement and optimisation of the methodology; Section 2.9 presents the microscope analysis of the different printing settings that are used in the trial experimentation. The consideration of a complex pelvis geometry case where no discernible axes of symmetry exist is presented in Section 3, where the numerical evaluation using finite element models of the different proposed trial experimentation is undertaken followed by the actual physical-trial experimentation in Section 3.1. A Bland Altman statistical analysis is performed to assess the agreement between the finite element models and the synthetic composite bone. This is repeated to assess the agreement between the physical-trial experimentation and finally alternative methods of validation are presented. The discussion of the results and future ongoing work in the field are found in Section 4.

The aim of this work is twofold, firstly, establishing the foundations of a multi-scale theory by presenting the finite similitude approach as its zeroth-order case and stating the necessary definitions emphasising the role scaling effects (β-dependencies) play in the biomechanical experimentation under consideration. Secondly, gauge the extent to which the similitude approach can be applied in the field of biomechanics specifically experimentation consisting of validation of finite element models by means of digital image correlation. Previous studies focus on simple geometries where axes of symmetry are present, therefore its applicability in a wider range of complex geometries where no discernible axes of symmetry exist provides increasing evidence of the success of the approach. This establishes the methodology and foundations of future work in patient-specific geometries and a multi-scale approach to scaled biomechanical experimentation. The main objective is to solve the plethora of obstacles that biomechanical research has to overcome, in this case, the availability of resources and the high cost.

2 Zeroth-Order Finite Similitude in Biomechanics

Reference[13] establishes the foundations for the use of finite similitude in the field of biomechanical experimentation; following the methodology, the main concern of the approach is the characterisation of the "deformation" of space. This characterisation is achieved through the map $\mathbf{x}_1 \mapsto \mathbf{x}_\beta$, which relates coordinate functions in orthonormal inertial frames and in differential terms takes the form $d\mathbf{x}_\beta = \mathbf{F} d\mathbf{x}_1$, which is interpreted as relating individual coordinate components of the coordinate system as $dx^i_\beta = F^i{}_j dx^j_1$; $\beta > 0$ is a length-scale parameter that quantifies the extent of the scaling involved. In the classical Newtonian frame, absolute time is also assumed to apply, represented in differential terms by the equation $dt_\beta = g(\beta) dt_1$, where both $g(\beta)$ and F are taken to be both spatially and temporally invariant.

The focus of the similitude approach is on space and the transfer of physical quantities through a region of space. It follows that in the physical space a control volume Ω^*_1 is necessary for the definition of similitude (for the control volume theory see reference[14]), where the subscript notation "1" refers to the physical space. The motion of the control volume Ω^*_1 is described with the diffeomorphism $\kappa_1 : \Omega^* \longrightarrow \Omega^*_1$ where Ω^* is a reference control volume. From this, the control volume velocity is defined as $\mathbf{v}^*_1 = \frac{D^*\kappa_1}{D^* t_1}$ where $\frac{D^*}{D^* t_1} = \frac{\partial}{\partial t_1}\Big|_{\mathbf{x}^*}$ is the control-volume derivative, and where $\mathbf{x}^* \in \Omega^*$. Analogously, the same construction can be invoked for the trial space with the subscript notation "β" replacing "1".

Space distortion arises on consideration of the notion of deformation in continuum mechanics applied to the space itself. Geometric measures (i.e. area and volume) between the two spaces can be related through Nanson's geometric identities, which takes the form $d\Gamma_\beta \mathbf{n}_\beta = d\Gamma_1 J \mathbf{F}^{-T} \mathbf{n}_1$ and volume $dV_\beta = J dV_1$, where $J = \det \mathbf{F}$. The Jacobian matrix $\mathbf{F}$, which describes space scaling has components defined by $F_{ij} = \frac{\partial x^i_\beta}{\partial x^j_1}$. The definition of Theorem 2.1 in reference[14] can be used to formulate a general expression of a balance law in transport form for a specific scalar or vector property $\Psi(1)$ associated to the motion of the control-volume with its derivative definition,

$$\frac{D^*}{D^*t_1}\int_{\Omega_1^*}\rho(1)\Psi(1)dV_1+\int_{\partial\Omega_1^*}\rho(1)\Psi(1)(\mathbf{v}(1)-\mathbf{v}^*(1))\cdot\mathbf{n}_1 d\Gamma_1 = \\ -\int_{\partial\Omega_1^*}\underline{\underline{J}}^{\psi}(1)\cdot\mathbf{n}_1 d\Gamma_1+\int_{\Omega_1^*}\rho(1)\mathbf{b}^{\psi}(1)dV_1 \quad (1)$$

where $\underline{\underline{J}}^{\psi}(1)$ is a "flux" term, $\mathbf{b}^{\psi}(1)$ is the source term, $\partial\Omega_1^*$ is the orientable boundary for Ω_1^*, $\mathbf{n}_1$ is an outward pointing unit normal on $\partial\Omega_1^*$, $\mathbf{v}(1)$ the velocity field and $\rho(1)$ is density. Analogously, the corresponding expression for the trial space control volume is

$$\frac{D^*}{D^*t_\beta}\int_{\Omega_\beta^*}\rho(\beta)\Psi(\beta)dV_\beta+\int_{\partial\Omega_\beta^*}\rho(\beta)\Psi(\beta)(\mathbf{v}(\beta)-\mathbf{v}^*(\beta))\cdot\mathbf{n}_\beta d\Gamma_\beta = \\ -\int_{\partial\Omega_\beta^*}\underline{\underline{J}}^{\psi}(\beta)\cdot\mathbf{n}_\beta d\Gamma_\beta+\int_{\Omega_\beta^*}\rho_\beta\mathbf{b}^{\psi}(\beta)dV_\beta. \quad (2)$$

where it is understood that Eqs. (1) and (2) are presently unrelated. The notation used for these properties emphasises the β-dependency of each quantity.

2.1 Isotropic Scaling

Focus in this paper is on isotropic scaling where $\mathbf{F}$ takes on the simplified form

$$\mathbf{F}=\beta\mathbf{I} \quad (3)$$

where $\mathbf{I}$ is the identity matrix/tensor and the Jacobian $J=\det\mathbf{F}=\beta^3$.

The process for relating transport equations (1) and (2) is by means of the deformation tensor $\mathbf{F}$ through the application of Nanson's identities $d\Gamma_\beta\mathbf{n}_\beta=d\Gamma_1\beta^2\mathbf{n}_1$ and $dV_\beta=\beta^3dV_1$ for isotropic scaling, which provides

$$\alpha_0^{\Psi}T_0^{\Psi}(\beta)=\frac{D^*}{D^*t_1}\int_{\Omega_1^*}\alpha_0^{\Psi}(\beta)\rho(\beta)\Psi(\beta)\beta^3dV_1+\int_{\partial\Omega_1^*}\alpha_0^{\Psi}(\beta)\rho(\beta)\beta^3\Psi(\beta)(g(\beta)\beta^{-1}\mathbf{v}(\beta)-g(\beta)\beta^{-1}\mathbf{v}^*(\beta))\cdot\mathbf{n}_1d\Gamma_1 \\ +\int_{\partial\Omega_1^*}\alpha_0^{\Psi}(\beta)g(\beta)\beta^2\underline{\underline{J}}^{\psi}(\beta)\cdot\mathbf{n}_1d\Gamma_1-\int_{\Omega_1^*}\alpha_0^{\Psi}(\beta)g(\beta)\beta^3\rho(\beta)\mathbf{b}^{\psi}(\beta)dV_1=0. \quad (4)$$

where Eq. (2) has been multiplied throughout by $g(\beta)$ and scaling parameter $\alpha_0^{\Psi}(\beta)$ to arrive at Eq. (4).

Eq. (4) is of fundamental importance and is effectively Eq. (2) but represented on the physical space and consequently captures all scale dependencies. Geometrical dependencies are explicitly visible with the presence of β^3 and β^2 terms but other $\beta-$dependencies are implicit in the fields, fluxes and sources. Relating the notation of Reference[13] it is assumed that $\Psi(1) = \Psi_{ps}$, $\rho(1) = \rho_{ps}$, $\mathbf{v}(1) = \mathbf{v}_{ps}$, $\underline{\underline{J}}^{\psi}(1) = \underline{\underline{J}}^{\psi}_{ps}$ and $\mathbf{b}^{\psi}(1) = \mathbf{b}^{\psi}_{ps}$ and similarly $\alpha_0^{\Psi}(1) = 1$, $g(1) = 1$ to facilitate Eq. (4) being identically equal to Eq. (1) for $\beta = 1$.

The issue in finite-similitude scaling theory is the revealing of implicit $\beta-$dependencies, which can be achieved in a number of ways but the focus in this paper is on the identity

$$\frac{d}{d\beta}(\alpha_0^{\Psi} T_0^{\Psi}) \equiv 0 \tag{5}$$

where "$\equiv$" means identically zero, which effectively means that there are no β terms present in the integrands in Eq. (4). This identity which underpins the finite similitude approach is now termed zeroth-order finite similitude and forms the zeroth-order case in a multi-scale approach not presented here.

The purpose of the scalars $\alpha_0^{\Psi}(\beta)$ are revealed by this identity as they are set to annihilate (where possible) the β terms that appear in the integrands in Eq. (4). It is evident that for all the integrands to be absent of β it is necessary and sufficient that corresponding terms in Eqs. (1) and (4) match, which means that the following identities must hold:

$$\rho(1)\Psi(1) = \alpha_0^{\Psi}(\beta)\beta^3\rho(\beta)\Psi(\beta) \tag{6a}$$

$$\mathbf{v}(1) - \mathbf{v}^*(1) = g(\beta)\beta^{-1}(\mathbf{v}(\beta) - \mathbf{v}^*(\beta)) \tag{6b}$$

$$\underline{\underline{J}}^{\Psi}(1) = \alpha_0^{\Psi}(\beta)g(\beta)\beta^2\underline{\underline{J}}^{\Psi}(\beta) \tag{6c}$$

$$\rho(1)\mathbf{b}^{\psi}(1) = \alpha_0^{\Psi}(\beta)g(\beta)\beta^3\rho(\beta)\mathbf{b}^{\psi}(\beta). \tag{6d}$$

For the biomechanical experimentation under consideration the main focus is the measurement of strain at bone surfaces and consequently the transport laws for momentum and

movement are of principal interest. The conservation of volume is typically absent in continuum mechanics (having no associated field) but it plays a part in finite similitude and is included in the analysis.

Since the physical space material properties consist of a trabecular and cortical material for the synthetic composite bone, the material properties are considered as a piecewise-constant function using the superscript "t" for trabecular and "c" for the cortical.

2.2 Scaling of Volume

For the conservation of volume $\Psi = \rho^{-1}$ and no flux or sink terms exist therefore the scaling relationships obtained from Eq. (6) are $1 = \alpha_0^1(\beta)\beta^3$ and $\mathbf{v}^*(1) = g(\beta)\beta^{-1}\mathbf{v}^*(\beta)$. It is evident that setting $\alpha_0^1(\beta) = \beta^{-3}$ has the effect of removing β from the transport equation for volume and ensures that Eq. (5) is satisfied. Note also that the relationship $\mathbf{v}^*(1) = g(\beta)\beta^{-1}\mathbf{v}^*(\beta)$ synchronises the movements of the control volumes, which is surely needed for scaled analysis and more on this can be found in reference[12].

2.3 Scaling of Mass

The conservation of mass is described on setting $\Psi \equiv 1$, $J^\Psi = 0$ since there is no flux term at the boundary and $\mathbf{b}^\Psi = \mathbf{0}$ as no source exists. From Eq. (6) the following useful expression is obtained:

$$\rho(1) = \alpha_0^\rho(\beta)\beta^3\rho(\beta). \tag{7}$$

where it can be observed that identical densities in the trial and physical spaces is possible on setting $\alpha_0^\rho(\beta) = \beta^{-3}$.

Recall that the density ρ is assumed to depend on β in a continuous fashion and that $\rho(1) = \rho_{ps}$ and through the parameter $\alpha_0^\rho(\beta)$ (which itself depends on β) a degree of material selection is possible. It is important to appreciate that the satisfaction of Eq. (7) is necessary to ensure the removal of β from the transport equation for mass so that Eq. (5) is satisfied. Note that in view of the relationship $\mathbf{v}^*(1) = g(\beta)\beta^{-1}\mathbf{v}^*(\beta)$ arising from conservation of

volume it immediately follows from Eq. (6b) that material velocity must satisfy $\mathbf{v}(1) = g(\beta)\beta^{-1}\mathbf{v}(\beta)$ in order for Eq. (5) to be satisfied.

In view of the spatially distinct properties of trabecular and cortical bone and the piecewise representation of material properties and since deformation of space has been characterised by one of the materials it is apparent that the main concern when dealing with more than one material is the preservation of the ratios between material properties. In this case

$$\frac{(\rho(\beta))^c}{(\rho(\beta))^t} = \frac{(\rho(1))^c}{(\rho(1))^t} \tag{8}$$

imposing further constraints on the remaining balance laws.

2.4 Scaling of Momentum

With the restriction of density and the synchronicity of the control-volume movement $\mathbf{v}^*(1) = g(\beta)\beta^{-1}\mathbf{v}^*(\beta)$ and its impact on material velocity (i.e. $\mathbf{v}(1) = g(\beta)\beta^{-1}\mathbf{v}(\beta)$), the balance law for momentum is considered particularly constricting, since velocity is the principal field, i.e. $\Psi = \mathbf{v}$. Using (6a) it is possible to derive the expression $\rho(1)\mathbf{v}(1) = \alpha_0^\nu(\beta)\beta^3\rho(\beta)\mathbf{v}(\beta)$ which, along with Eq. (7), results in the following expression for the scaling parameter $\alpha_0^\nu(\beta)$

$$\alpha_0^\nu(\beta) = \alpha_0^\rho(\beta)g(\beta)\beta^{-1} \tag{9}$$

confirming that $\alpha_0^\nu(\beta)$ is not a free parameter and whose value is influenced by the time-scaling parameter $g(\beta)$.

Equations (6c), (6d) also give the relations

$$\underline{\underline{\sigma}}(1) = \alpha_0^\nu(\beta)g(\beta)\beta^2\underline{\underline{\sigma}}(\beta) \tag{10}$$

$$\rho(1)\mathbf{b}^\nu(1) = \alpha_0^\nu(\beta)g(\beta)\beta^3\rho(\beta)\mathbf{b}^\nu(\beta) \tag{11}$$

where the stress tensor relationship arises from the "momentum flux" (i.e. force) in the momentum transport equation.

Note that $\underline{\underline{\sigma}}(\beta)$ and $\mathbf{b}^\nu(\beta)$ are dependent on β and it is the requirement that Eq. (5) is satisfied that reveals precisely the nature of these dependencies. The value for $\alpha_0^\nu(\beta)$ can be

determined on specification of $g(\beta)$ on the basis of the constitutive response of Eq. (10). As in reference[13], it is restricted to a linear-elastic material responses.

2.5 Scaling of Movement

Prior to examination of material constitutive behaviour it is necessary first to ascertain the effect scaling has on displacement and consequently strain. Introduced in Reference[14] is the transport equation for movement, where the displacement field $\mathbf{u}$ is constrained. Application of Eq. (6a) for movement provides the similarity condition $\rho(1)\mathbf{u}(1) = \alpha_0^u(\beta)\beta^3\rho(\beta)\mathbf{u}(\beta)$, which on substitution of Eq. (7) reduces to

$$\alpha_0^\rho(\beta)\mathbf{u}(1) = \alpha_0^u(\beta)\mathbf{u}(\beta). \tag{12}$$

Note that using the source term identity Eq. (6d) yields $\rho(1)\mathbf{v}(1) = \alpha_0^u(\beta)g(\beta)\beta^3\rho(\beta)\mathbf{v}(\beta)$, which after substitution of Eq. (7) gives $\alpha_0^\rho(\beta)\mathbf{v}(1) = \alpha_0^u g(\beta)\mathbf{v}(\beta)$. However, continuity and momentum provided the relationship $\mathbf{v}(1) = g(\beta)\beta^{-1}\mathbf{v}(\beta)$ for material velocity and consequently

$$g(\beta)\alpha_0^u(\beta) = \alpha_0^\nu(\beta) = \alpha_0^\rho(\beta)g(\beta)\beta^{-1} \tag{13}$$

and it immediately follows from Eq. (12) that $\mathbf{u}(1) = \mathbf{u}(\beta)\beta^{-1}$.

Note that $\alpha_0^u(\beta)$ is not a free parameter being related to $\alpha_0^\nu(\beta)$ but such a constraint cannot be too surprising in view of the intrinsic relationship between velocity and displacement. Upon differentiation of $\mathbf{u}(1) = \mathbf{u}(\beta)\beta^{-1}$ with respect to time and taking into account the relationship $dt_\beta = gdt_1$ provides consistently the velocity relationship $\mathbf{v}(1) = g(\beta)\beta^{-1}\mathbf{v}(\beta)$. The two relationships $dx_\beta^i = \beta dx_1^i$ and $du_\beta^i = \beta du_1^i$ provide the strain tensorial identity $\underline{\underline{\epsilon}}(\beta) = \underline{\underline{\epsilon}}(1) \quad \forall\beta$, which means that strain $\underline{\underline{\epsilon}}(\beta)$ does not vary with β. It is important to emphasise that all constraints on field variables with scale are simply down to the underpinning constraint provided by identity Eq. (5).

2.6 Constitutive response

Synthetic composite bone is reported as transversely orthotropic; however sources (see reference[9]) using DIC as means of validating FE models commonly consider the synthetic composite bone as linear-isotropic elastic homogeneous material. This is particularly the case when dealing with complex geometries such as the pelvic bone where no clear axes of symmetry can be discerned. Therefore on substitution of Hooke's linear stress-strain (for isotropic materials) relationships into Eq. (10) the following is obtained

$$\frac{E(1)}{1+\nu(1)}\left[\epsilon_{ij}+\frac{\nu(1)}{1-2\nu(1)}\epsilon_{kk}\delta_{ij}\right]=\alpha_0^{\nu}(\beta)g(\beta)\beta^2\frac{E(\beta)}{1+\nu(\beta)}\left[\epsilon_{ij}+\frac{\nu(\beta)}{1-2\nu(\beta)}\epsilon_{kk}\delta_{ij}\right]. \tag{14}$$

where the β-dependency of the strains has been dropped in view of it being constant throughout the scales since the displacement identity revealed its invariance with respect to β.

This equation can be readily satisfied with the assumption that Poisson's ratio $\nu(\beta)$ is also considered independent of β. This requirement places a restriction on the types of 3D printed materials that can be used. Although this requirement may not necessarily be achievable in practice, the element of experimental design nevertheless allows for its approximate implementation. Note that since constitutive relationships are explicitly stated the success or failure of the approximation is made apparent in any physical trial-material test. With this constraint Eq. (14) reduces to,

$$E(1)=\alpha_0^{\nu}(\beta)g(\beta)\beta^2E(\beta) \tag{15}$$

where on substitution of Eq. (9) and on rearrangement provides,

$$g(\beta)=\sqrt{\frac{E(1)}{\beta\alpha_0^{\rho}(\beta)E(\beta)}} \tag{16}$$

where $g(\beta)$ relates the timing of any two physical experiments (i.e. full and scaled); note that even for quasi-static studies, finite-similitude relates physical trials and hence requires information on the timings involved in said trials.

In this work Young's modulus is considered to be a spatially piece-wise function, which yields and analogous result to Eq. (8), i.e.

$$\frac{(E(\beta))^c}{(E(\beta))^t} = \frac{(E(1))^c}{(E(1))^t} \tag{17}$$

which constrains the value of the trabecular modulus $(E(1))^t$ as in the previously mentioned case of density.

Relationships for stress can be used to determine relationships for force, since in the physical space $dF(1) = \underline{\underline{\sigma}}(1) \cdot \mathbf{n}_1 d\Gamma_1$ and recall that $d\Gamma_\beta \mathbf{n}_\beta = d\Gamma_1 \beta^2 \mathbf{n}_1$. Integration over a planar surface provides the force relationship

$$F(1) = \alpha_0^\nu(\beta) g(\beta) F(\beta) \tag{18}$$

which is in accordance with the operations applied to Eq. (2) for momentum, i.e. multiplication by $g(\beta)$ and $\alpha_0^\nu(\beta)$.

It is apparent that the zeroth-order approach provides the relationships for scaling and the characterisation of space explicitly stated, which is a clear advantage of the approach. The ability to apply scaling in either direction is another important advantage. This construction is based on the use of the scaling map and since the map $\mathbf{x}_1 \mapsto \mathbf{x}_\beta$ is a diffeomorphism, the same construction can be made using the inverse of the map, i.e. $\mathbf{x}_\beta \mapsto \mathbf{x}_1$. This results in two virtual spaces (direct-scaling and reverse-scaling material models) that can be used to compare the results in their respective spaces as shown in Figure 1. Another advantage particular to the approach that can be easily implemented using commercial finite element software. As presented in this work the notation and definitions serve as the zeroth case of a multi-scale theory where the scaling effects and β-dependencies are clearly stated.

[Figure 1 about here.]

2.7 Summary of Zeroth-Order Finite Similitude Theory

The finite similitude theory is founded on the metaphysical concept of space deformation by means of a characterising scaling map between the physical and trial spaces. The zeroth-order

theory involves the matching of projected trial-space transport equations with corresponding equations in the physical space. Similarity equations are returned, which when satisfied guarantee that the proposed trial experiment conforms to the behaviour of the system in the physical space. The space deformation map facilitates the creation of virtual models in both spaces and enables comparison between experimental results or representative finite-element models. The practical application of the novel scaling approach can be summarised as such:

- *Characterisation of the Deformation of Space*: the zeroth-order Eq. (5) is an assumed global length-scale invariance that returns similarity conditions on relating projected trial and physical transport equations.

- *Similarity Conditions*: degrees of freedom exist in the similarity conditions in the form of scaling parameters, which can be set by matching some aspect of the constitutive response of the materials involved.

- *Trial Space Experimental Design*: using the aforementioned relationships for scaling the choice of trial space materials is undertaken, which entails the experimental design aspect of the approach.

- *Comparison of Experimental Behaviours*: using the virtual spaces obtained by means of the similitude approach (direct and reverse scaling) a comparison between physical behaviours can be performed to assess the success and applicability of the approach.

2.8 Trial Space Materials

Advancements in 3D printing technology allows for the fast prototyping and manufacturing of complex geometries using cheap polymers that are easily available to model synthetic composite bone, more specifically fourth-generation composite bone (reference [15]), solving the two main concerns that arise in biomechanical experimentation. Reference [13] provides a first approach for a simple and femur geometry however the aim of this work is the optimisation and advancement of the approach and to illustrate its applicability in realistic biomechanical

experimentation. Recent improvements in the 3D printing software allows for a closer match of the density, thus the interface between materials can now be analysed using a laser scanning microscope.

The exterior material proposed for the trial space is PLA (Polylactic Acid) due to its previous success in scaled experimentation. The principal concern is matching the elastic modulus, reference[16] provides a detailed analysis of the expected elastic modulus that corresponds to a specific printing setting.

Using the direct scaling material properties (virtual trial space) as guidance for experimental design, TPU (Thermoplastic Polyurethane) flexible filaments with Shore hardness 90A, 93A and 95A were selected for the trabecular material. Using the relationship between Shore hardness and Young's modulus by Gent[17] an estimate of the interior material elastic modulus in the trial space is obtained.

$$E(\beta) = \frac{0.0981(56 + 7.66s(\beta))}{0.137505(254 - 2.54s(\beta))} \tag{19}$$

where $s(\beta)$ is the Shore hardness.

While previous attempts focused solely on the elastic modulus it is possible to obtain a closer match for the density using a 30% infill density in the printing setting for the trabecular material. All of the scaling parameters and material properties for the trial and physical spaces including their respective virtual spaces are shown in Table 1.

[Table 1 about here.]

2.9 Microscope Analysis of Materials

The comparison between the physical and trial material's micro-structure (including bone samples) is undertaken with the objective of gauging the extent to which specimens proposed for the trial space resemble the structure of the physical space materials. Cortical and trabecular bone have specific properties that can only be described at the microscale and whilst the scaling approach does not attempt to replicate the physics at the microscale it

is necessary to guarantee that the behaviour of the printed materials is not significantly different. The comparison is performed with different 3D printing settings to optimise the methodology and compare them against bone and synthetic composite bone samples, the 3D printed cylinder samples consisted of PLA/TPU 95A with a 30% trabecular infill and 0.2mm layer height and different merge settings: no overlap = 0 mm, small overlap = 0.1875 mm, large overlap = 1.045 mm and minimised wall overlap = 2 line width trabecular wall with 0.728 mm overlap. Table 2 shows the comparison between the 3D images taken using a confocal laser scanning microscope (Keyence X200K 3D laser microscope).

[Table 2 about here.]

The images show a gradual change for the bone sample whereas the synthetic composite bone shows a stark contrast between the materials, the small overlap and the minimised trabecular wall overlap resembles bone more closely due to the slight gradual interface between materials. An important consideration when dealing with more than one material, especially in biomechanics, is the bonding between materials or the characterisation of the interface which provides means to quantify the difference between them. The parameters used for the characterisation are:

- Arithmetical mean height (**Sa**), *the mean of the absolute value of the height of points within the defined area.*
- Developed interfacial area ratio (**Sdr**), *the percentage of the definition area's additional surface area contributed by the texture as compared to the planar definition area.*
- Root mean square height (**Sq**), *represents the root mean square value of ordinate values within the definition area (standard deviation of heights).*
- Skewness (**Ssk**), *represents the degree of bias of the roughness shape (asperity).*
- Kurtosis (**Sku**), *measures the sharpness of the roughness profile.*
- Maximum peak height (**Sp**), *the height of the highest peak within the defined area.*

- Maximum pit height (**Sv**), *the absolute value of height of the lowest pit within the defined area.*

- Root mean square gradient (**Sdq**), *root mean square of slopes at all points in the definition area.*

- Density of peaks (**Spd**), *number of peaks per unit area.*

[Table 3 about here.]

Table 3 shows the microscope results for each sample. The parameters were compared against the bone results (b_i) using an equivalent expression of the norm of a vector in which each component is the error of the specific setting (and synthetic composite bone), the expression can be written as such

$$E_n = \sum_{i=1}^{n} \left(\frac{(x_i - b_i)}{b_i}\right)^2 \tag{20}$$

where $n = 9$ corresponding to the total number of parameters, and where x_i is the corresponding sample that is used for comparison.

The results show that for the parameters considered the small overlap resembles the interface between cortical and trabecular bone more closely.

3 Pelvis Physical-Trial Experiment Analysis

The use of finite element models when analysing problems specifically in the case of the hemipelvis has yielded important results and has become more widespread in recent years (references[9],[7],[8],[18]). The consideration of a left hemi-pevis complex geometry extends the application of the approach with the aim of improving upon previous iterations of the application and even providing foundations to validate future experimentation in geometries that are more complex than what standardised synthetic composite bones can solve such as patient specific geometries, variable densities for the trabecular material, etc.

An advantage of the zeroth-order approach is the ability to use finite element models to assess the projected success of the approach by comparing the finite element results in the physical space and the virtual physical space (using reverse-scaling material properties) or the trial space with its respective virtual trial space (direct-scaling material properties) before the actual physical-trial experimentation. Two models are constructed (physical and trial spaces), the comparison is made in the physical space but the same results are obtained for the trial space since both comparisons are equivalent in this case. The boundary conditions are set as encastre in the sacroiliac joint and the pubic symphysis. A portion of a femoral head is considered to apply the contact force in the acetabular cup. The different tests are considered quasi-statically loaded for the purpose of finite-element analysis. The material properties of the physical space model and reverse-scaling were taken from Table 1.

[Figure 2 about here.]

Figure 2 shows the boundary condition with the viewpoints of XZ and ZY (respectively), the regions highlighted for the sacroiliac joint and the pubis symphysis contact are constrained by an encastre (displacements and rotations in all directions were defined as zero). The loads are applied using the values in the literature (including the angle made by the load and the contacting pubis symphysis support) for the one-leg standing position (References[19],[9]) thus an increasing force from 1200 N to 2000N (with 100 N increments) is applied in the FE models.

The refined mesh consists of 320,519 elements for the hemipelvis and 18,710 for the femoral head, which results in a total of 339,229 elements. These are based on the boundary conditions given in reference[9], which provides the general methodology for validation of a pelvis finite-element model. Not considered in reference[9] however is the application of a Bland-Altman statistical analysis, which is needed when analysing the agreement between finite element models and the physical experimentation.

[Figure 3 about here.]

The surface region used for comparison is highlighted in Figure 3, the region is larger than the region of interest that would be expected to measure in the actual physical-trial experimentation. The comparison is made node-to-node using the same mesh in the physical space, a total of 14,615 nodes were compared. The strain measurements are essentially coordinate dependent however it is possible to obtain independent values using the eigenvalues λ_i of the stretch tensor. The digital image correlation optical measurement technique used in the actual physical-trial experiments is constrained by the surface (two-dimensional) however it is still possible to deduce a three-dimensional measurement. From the two-dimensional measurement of the eigenvalues λ_1, λ_2 the major strain φ_1 and minor strain φ_2 (larger and smaller value respectively) can be obtained, assuming volume constancy defined as

$$\lambda_1 \cdot \lambda_2 \cdot \lambda_3 = 1 \tag{21}$$

which for this particular case of biomechanical experimentation holds true.

Criteria taking this into account prove useful to overcome the practical constraints of coordinate systems and are readily available when choosing the output in the digital image correlation software. Consequently the comparison in the preliminary finite element models (assisted by the virtual spaces) is made using the von Mises equivalent strain. The effective strains according to the von Mises equivalent strain[20] results from the following formula:

$$\varphi_{eq} = \sqrt{\frac{2}{3}(\varphi_1^2 + \varphi_2^2 + \varphi_3^2)} \tag{22}$$

where φ refers to the logarithmic strain or true strain ($\epsilon = e^{\varphi}$).

An additional advantage of the von Mises expression is the consideration of all strain components resulting in an improved measurement of small strain values which can become problematic in the biomechanical experiment under consideration due to the small deformations of bones caused by peak loads in human bones[19]. The small deformations caused by the peak forces guarantee that in the case of synthetic composite bone and the proposed trial space materials, the assumed linear-elastic response of the materials is obeyed.

The average percentage error (surface strain) across all the values of the force is less than

9.2% in the case of the PLA/TPU 95A and in the case of the PLA/TPU 90A it is less than 15.3%; note that the combination of materials PLA/TPU 93A is considered identical since the percentage error is less than 0.0001%.

[Figure 4 about here.]

These results provide a first indication that the PLA/TPU 95A and PLA/TPU 93A combinations of materials for the actual physical-trial experimentation yields the most reliable results to confirm the use of these 3D printing materials for the trial experimentation. The combination of materials PLA/TPU 90A has a percentage error of 15.3% which can possibly result in surface strain measurements too high to obtain a good agreement and thus is discarded for the physical-trial experimentation. In the case of the material combination PLA/TPU 95A the average value of strain is 800 micro-strains thus the average percentage error of 9.2% (73 micro-strains) is less than the reported accuracy of 100 micro-strains for the 5M (5 megapixel) configuration of the digital image correlation system's manufacturer using the parameters stated in Table 6 of Appendix B, therefore it is deemed acceptable for the experimentation under consideration. This is a clear advantage of the zeroth-order finite similitude approach since the use of reverse-scaling material properties and finite element models provide a quick assessment of the approach before any experimentation takes place which also results in a reduced cost of experimentation and assists the design element of the scaling approach.

3.1 Physical-Trial Experimentation

The physical-trial experimentation was undertaken for the left hemipelvis using the combination of material properties PLA/TPU 95A and PLA/TPU 93A for the trial space. The experimental work was carried out with the aim of assessing the applicability of the finite similitude approach in a wider range of experiments using the optimised settings to improve upon previous iterations of the approach. The same experimentation was used to validate

the FE models used for comparison to ensure the physical-trial experimentation results were consistent with the numerical results.

3.1.1 Experimental Setup

The load was applied using a single column universal testing machine (Instron 3344) using a 2 KN load cell to which the 50mm and 36mm steel ball bearing was attached for the physical and trial experimentation respectively. The hemipelvis was clamped to a holding device fixing the sacroiliac joint and supporting the pubis symphysis. The DIC system used for the deformation measurements and vertical surface strain measurements consisted of an array of two 5-megapixel cameras, a focal length of 12 mm was utilised. The experimental setup is shown in Figure 5.

[Figure 5 about here.]

The same experimental set up was used for the physical-trial experimentation using the same load and constraints as in the finite element models. Figure 6 shows the comparison between the experimental setup and the finite element boundary conditions.

[Figure 6 about here.]

The contact area between the models and physical experimentation was compared to ensure the femoral head and the acetabulum had the same contact areas in the finite element models replicating the experimental set up and thus confirming the reliability of the results. It can be observed in Figure 7 the contact areas in the physical experimentation and in the finite element models show a similar pattern.

[Figure 7 about here.]

The force values in the physical space range from 1200 N to 1800 N with 200 N increments consistent with the average peak loads in a one-leg standing. The reported accuracy of the

digital image correlation measurements and practical purposes restricts the measurement to increments of 200 N instead of the values used in the finite element analysis (the maximum force applied on the machine is less than 2000 N, thus that value was not considered); the hemipelves were removed and retested every time to emulate different subjects. The load was applied until the load cell output was in equilibrium to avoid any relaxation behaviour during the recording of images, the parameter g can be used to assess the time difference between spaces for this to occur however the consideration of a quasi-static experiment renders this unnecessary (it is only required to wait for equilibrium to be achieved in either space). The trial space force values were calculated using Eq. (18) which results in 155.2 N to 232.7 N with 25.9 N increments for the PLA/TPU 93A and 159.9 N to 239.7 N with 26.6 N increments for PLA/TPU 95A.

3.1.2 Data Processing

The experiment is considered quasi-static thus the digital image correlation software records images at each loading stage (one stage-test for each value of the force) and consequently calculates strain values in the surface for each value of force displaying the von Mises equivalent strain as the quantity of interest. As a result of the coordinate-independent criteria the visualisation pattern does not require matching of coordinate systems for comparison, Figure 8 shows the superimposed images of the computation mask with the applied post-filtering over the photograph taken at stage 1 in the left camera compared to the same photograph with the superimposed finite element model surface which shows the two measurement techniques yield similar results within the region used for measurement. To quantify the mismatch between visualisation strain patterns that arise from the measurement error, the results are analysed in the statistical data of the software using the average of the von Mises equivalent strain in the region selected after the data from the computation mask has been processed. In cases where some glare was observed in the region of interest as can be shown in Figure 8, to account for the missing subsets, the image of the measured surface was superimposed to the finite element model and each element face that corresponded to the missing subset was

omitted from the comparison. In the case of the comparison between synthetic composite bone and 3D printed materials the same regions were selected omitting any subsets with poorly correlated data.

[Figure 8 about here.]

3.1.3 Results

A Bland-Altman statistical analysis[6] was carried out for all of the tests, in this case the synthetic composite bone is regarded as the "gold standard". The repeatability assessment was first performed to assess whether a good agreement could be obtained. Ten measurements of strain were taken for each value of the force (in the physical space). The analysis of repeatability (replicated measurements on a sample of subjects) provides a good measure of the consistency and ability to obtain a good agreement because if poor repeatability is found then a poor agreement will follow in the Bland-Altman statistical analysis. The repeatability assessment encapsulates the error arising from all of the sources involved in the method of measurement as such it guarantees the systematic error of the digital image correlation measurement technique is within acceptable ranges to obtain a good agreement. The differences between each of the 10 measurements was compared against each other resulting in 180 measurements. The interpretation of the analysis in this case is that each pair of measurements corresponds to two measurements made to the same subject.

The within-subject repeatability is assumed to be independent since the standard deviation and the mean of the measurements of strain between replicates (repeated experiments on same specimen) shows no tendency to change with the magnitude of measurements, Table 4 shows the values for the repeatability assessment for the synthetic composite hemipelvis and the 3D printed hemipelves. Since the results are within the acceptable ranges as the coefficient of repeatability is less than 100 micro-strains which is the reported accuracy of the DIC measurements a Bland-Altman statistical analysis was carried out. Each measurement of the experiments was compared against the FE model predicted values, using the same interpretation where each pair (experimental, FE) is carried out in a single subject. The 95%

confidence interval of the statistical analysis is calculated assuming a normal distribution of the differences as a consequence of the subject interpretation (in this case being the same specimen used for experimentation) thus its variation is null, what is left is the measurement error. The error of the digital image correlation system depends on the measurement chain (lens, camera, loading cell calibration, stochastic spray pattern, DIC calibration, parameters, etc...) and each can be considered as a random variable independent of the other, invoking the Central Limit Theorem allows the assumption of a normal distribution for the measurement error and consequently the differences.

The statistical analysis is summarised in Table 4, the limits of agreement for the Sawbones hemipelvis are less than 100 micro-strains which is the reported accuracy of the DIC measurements. This shows good supporting evidence of a good agreement between the FE models and the Sawbones hemipelvis, the same analysis is carried out for the agreement between the composite bone and the PLA/TPU 93A and the PLA/TPU 95A. The limits of agreement are below or equal to the reported accuracy (100 micro-strains) thus showing a good agreement. While the upper limit of agreement between the synthetic composite hemipelvis and the material combination PLA/TPU 95A is 100 micro-strains, statistically, 95% of the differences between measurements are at or below this limit thus is considered acceptable and a good agreement for the purposes of the experimentation under consideration.

[Table 4 about here.]

This shows good supporting evidence for the applicability of the approach in the case of a complex pelvis geometry and gives insight to the broader applicability of the approach stated in reference[13]. Another interesting result is the ability to validate models using different techniques particular to the finite similitude approach, in this case the use of the trial-experimentation results to validate the FE models using the reverse scaling. While the Bland Altman approach has validated the measurement technique by showing a good

agreement between the physical-trial experimentation, it is possible to confirm this result by using the trial experimentation alone.

The Bland Altman statistical analysis was carried out to assess the agreement between the FE models (with the respective reversed scaled material properties) and the 3D printed hemipelves. One measurement of each experiment in the trial space was compared against one in the FE model (with the respective reverse-scaling material properties) using the same interpretation where each pair is carried out in a single subject. The statistical analysis is summarised in Table 4, the limits of agreement are within the acceptable ranges (below 100 micro-strains) thus showing supporting evidence of a good agreement for the two proposed measurement techniques. This result confirms that the validation of the FE models can be performed using the reverse-scaling material properties and the trial experimentation. It is important to note that the most straightforward way of validating the FE model is using the trial experimentation with the physical material properties since it has been shown to have a good agreement but the versatility of the approach allows these different ways of validation.

4 Conclusions

This work aims to gauge the success of the application of the zeroth-order finite similitude approach in bio-mechanical experimentation consisting of validation of finite element models in a wider range of complex geometries than previous iterations, as well as optimising and improving the methodology for scaling synthetic composite bone. In this case the complex geometry tested was a left hemipelvis with three different combinations of trial-space materials PLA/TPU 93A, PLA/TPU 95A and PLA/TPU 90A. The physical-trial experimentation was subsequently analysed for these materials with the exception of the material combination PLA/TPU 90A using isotropic scaling with the main objective of the trial experimentation being the reduction of the cost and the assistance of manufacturing techniques for rapid testing with easily obtained materials. The conclusions can be summarised as such:

- The approach has been optimised for the experimentation under consideration with

microscopic analysis and the advancement in 3D printing manufacturing technology. The comparison showed that for the surface parameters considered the interface between materials that more closely resembles bone are the 3D printed materials with the small overlap setting (0.1875mm) and the reverse-scaling of the density shows a closer match to the physical space material properties.

- The numerical results for the left hemipelvis showed that the average percentage error across all the values of the force is less than 9.2% in the case of the PLA/TPU 95A and in the case of the PLA/TPU 90A it is less than 15.3% with the combination of materials PLA/TPU 93A being identical (percentage error $< 0.0001\%$).

- The physical-trial experimentation for the combination of trial space materials PLA/TPU 93A and PLA/TPU 95A was analysed using a Bland Altman statistical analysis to assess the agreement between the different materials; the finite element models were validated using the same statistical analysis. The synthetic composite hemipelvis was shown to have a good agreement with the finite element models thus validating the model results, additionally the trial-space material combinations were shown to have a good agreement with the synthetic composite bone results.

- The analysis confirms the applicability of the scaling approach in more complex geometries with the selected trial materials as a viable alternative to synthetic composite bone for the validation of finite element models using digital image correlation software and serves as the foundation for further testing of complex geometries where presently no synthetic option for testing exists.

4.1 Future Work

The analysis of scaled experimentation for different scaling parameters β to gauge the extent to which the current approach is valid and whether any scale effects are present during experimentation, this also serves as the foundation of the analysis of high-order finite similitude, which is the natural extension of the zeroth-order approach performed in these experiments.

Having obtained good supporting evidence of the approach in the various complex geometries that have been standardised by the use of synthetic composite bone, it is now possible to assess the effectiveness of the approach for geometries that are not possible to obtain with synthetic composite bone. This is particularly useful in cases where patient specific geometries are required or different material properties such as varying bone density, an example of this can be found in the validation of models where osteoporosis is present since there is a potential for simulating osteoporotic bone by reducing the bone density of the trial space materials or the thickness of the cortical bone in the trial space; research into the feasibility of this approach is of interest in the field of biomechanics.

Conflict of Interest

The authors declare that they have no conflict of interest.

Acknowledgment

The authors would like to acknowledge the National Council of Science and Technology of Mexico for providing support for Raul Ochoa-Cabrero to facilitate his research at the University of Manchester.

Appendix A

The Bland Altman plots for each of the statistical analyses for the pertaining physical-trial experimentation tests and subsequent finite element model validation are included to support the results reported (table 5).

[Table 5 about here.]

Appendix B

The following table (6) contains the digital image correlation system measurement reporting requirements.

[Table 6 about here.]

References

1. Alessandro Casaburo, Giuseppe Petrone, Francesco Franco, and Sergio De Rosa. A review of similitude methods for structural engineering. *Applied Mechanics Review*, 71:030802, May 2019.

2. Juan M. Lirola, Estefana Castaneda, Benito Lauret, and Mohamed Khayet. A review on experimental research using scale models for buildings: Application and methodologies. *Energy and Buildings*, (147):72–110, March 2017.

3. Andrew J. Spence. Scaling in biology. *Current Biology*, Volume 19(2):R57–R61, January 2009.

4. Dan Dragomir-Daescu, Asghar Rezaei, Susheil Uthamaraj, Timothy Rossman, James T. Bronk, Mark Bolander, Vincent Lambert, Sean McEligot, Rachel Entwistle, Hugo Giambini, Iwona Jasiuk, Michael J. Yaszemski, and Lichun Lu. Proximal cadaveric femur preparation for fracture strength testing and quantitative ct-based finite element analysis. *Journal of Visualized Experiments*, 121, March 2017.

5. Cornelius T Leondes. *Biomechanical Systems Technology: Muscular Skeletal Systems*. World Scientific Publishing, 2009.

6. D. G. Altman and J. M. Bland. Measurement in medicine: the analysis of method comparison studies. *The Statistician*, 32:307–317, 1983.

7. Zhenmin Zou, Arturo Chavez-Arreola, Parthasarathi Mandal, Tim N. Board, and Teresa Alonso-Rasgado. Optimization of the position of the acetabulum in a ganz periacetabular osteotomy by finite element analysis. *Journal of Orthopeadic Research*, 31(3):472–479, March 2013.

8. Teresa Alonso-Rasgado, Jose F. Del-Valle-Mojica, David Jimenez-Cruz, Colin G. Bailey, and Tim N. Board. Cement interface and bone stress in total hip arthroplasty: Relationship to head size. *Journal of Orthopaedic Research*, pages 2966–2977, November 2018.

9. Rajesh Ghosh, Sanjay Gupta, Alexander Dickinson, and Martin Browne. Experimental validation of finite element models of intact and implanted composite hemipelvises using digital image correlation. *Journal of Biomedical Engineering*, 134(8):081003, August 2012.

10. P. W. Bridgman. *Dimensional Analysis*. Yale University Press, 1922.

11. G. I. Barenblatt. *Scaling, Self-Similarity, and Intermediate Asymptotics*. Cambridge University Press, 1996.

12. Keith Davey, Rooholamin Darvizeh, and Anees Al-Tamimi. Scaled metal forming experiments: a transport equation approach. *International Journal of Solids and Structures*, 125:184–205, July 2017.

13. Raul Ochoa-Cabrero, Teresa Alonso-Rasgado, and Keith Davey. Scaling in biomechanical experimentation: a finite similitude approach. *Journal of the Royal Society Interface*, 15(143):20189254, June 2018.

14. Keith Davey and Rooholamin Darvizeh. Neglected transport equations: extended rankine-hugoniot conditions and j-integrals for fracture. *Continuum Mechanics and Thermodynamics*, 28(5):1525–1552, March 2016.

15. Sawbones. *Biomechanical Test Materials*. A Division of Pacific Research laboratories, Inc., Malmo, Sweden, 2016.

16. B.M. Tymrak, M. Kreiger, and J.M. Pearce. Mechanical properties of components fabricated with open-source 3-d printers under realistic environmental conditions. *Materials and Design*, 58:242–246, 2014.

17. A.N. Gent. On the relation between indentation hardness and young's modulus. *Rubber Chemistry and Technology*, 31(4):896–906, 1958.

18. Jose F. Del-Valle-Mojica, Teresa Alonso-Rasgado, David Jimenez-Cruz, Colin G. Bailey, and Tim N. Board. Effect of femoral head size, subject weight, and activity level on acetabular cement mantle stress following total hip arthroplasty. *Journal of Orthopaedic Research*, pages 1771–1783, August 2019.

19. G. Bergmann, F. Graichen, A. Rohlmann, A. Bender, B. Heinlein, G. N. Duda, M. O. Heller, and M. M. Morlock. Realistic loads for testing hip implants. *Bio-Medical Materials and Engineering*, (20):65–75, 2010.

20. Aramis. *ARAMIS User Manual - Sofware*. GOM Optical Measuring Techniques, Braunschweig, Germany, 2007.

21. International Digital Image Correlation Society, Jones E. M. C., and Iadcola M. A. (Eds.). *A Good Practices Guide for Digital Image Correlation*. Albuquerque, New Mexico, United States of America, 2018. https://doi.org/10.32720/idics/gpg.ed1.

List of Figures

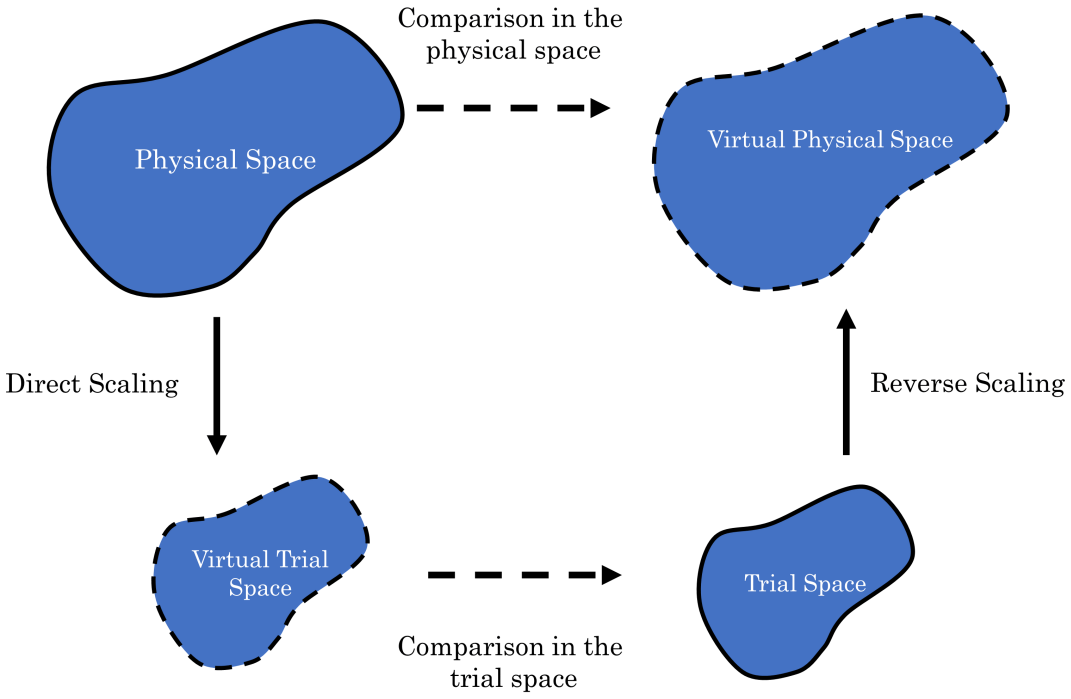

Figure 1: The figure shows the process of comparison in the finite similitude methodology using the scaling map and its inverse function (direct and reverse scaling respectively) where the representation of the virtual physical space (using the reverse scaling) allows for its comparison in the physical space and the direct scaling virtual space allows for the comparison in the trial space.

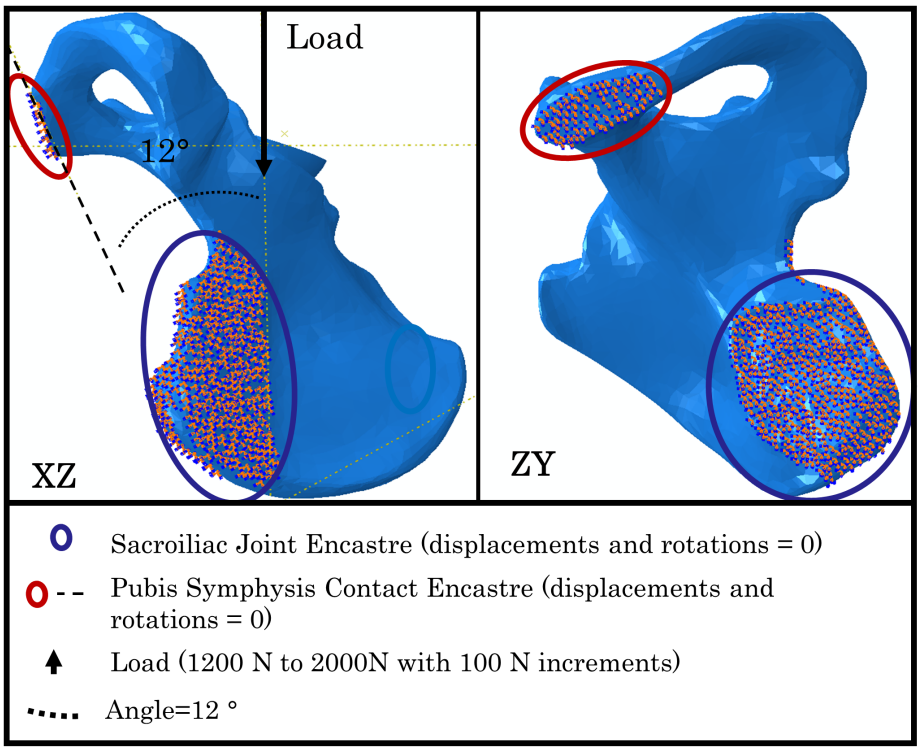

Figure 2: Left hemipelvis boundary conditions with the regions highlighted showing the sacroiliac joint and pubis symphysis contact which are constrained by an encastre where all displacements and rotations in all directions are zero. The loads applied are consistent with the literature ([9],[19]) for a one-leg standing position.

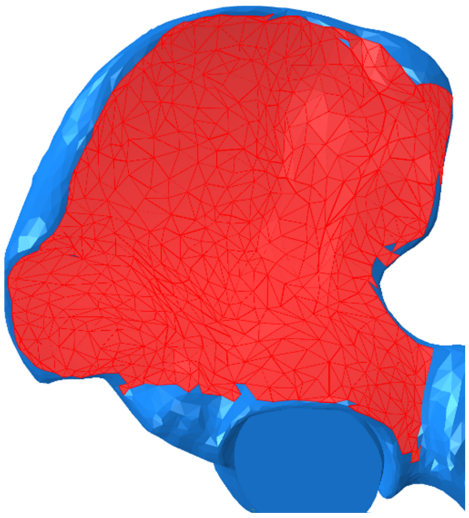

Figure 3: Region used for node-to-node comparison in the FE model, the surface strain is compared in the physical space using the reversed-scaled material properties. The area contains a total of 14,615 nodes used for comparison.

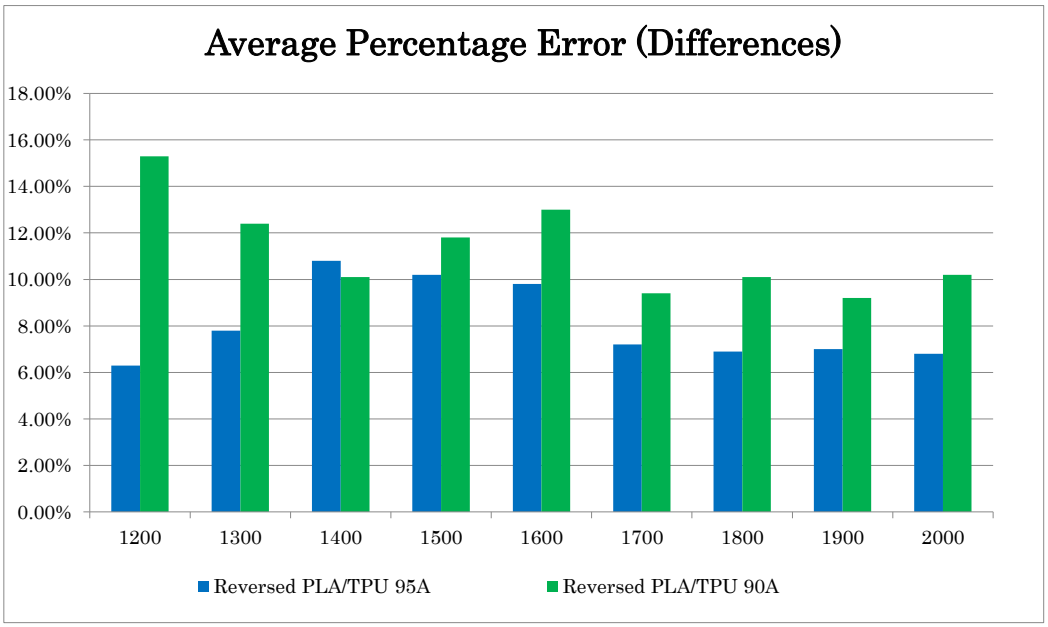

Figure 4: Comparison in the finite element models using the reverse scaling material properties of the trial space material combinations PLA/TPU 95A and PLA/TPU 90A in the physical space. The values show the percentage error for each value of the force applied ranging from 1200 N to 2000 N with 100 N increments.

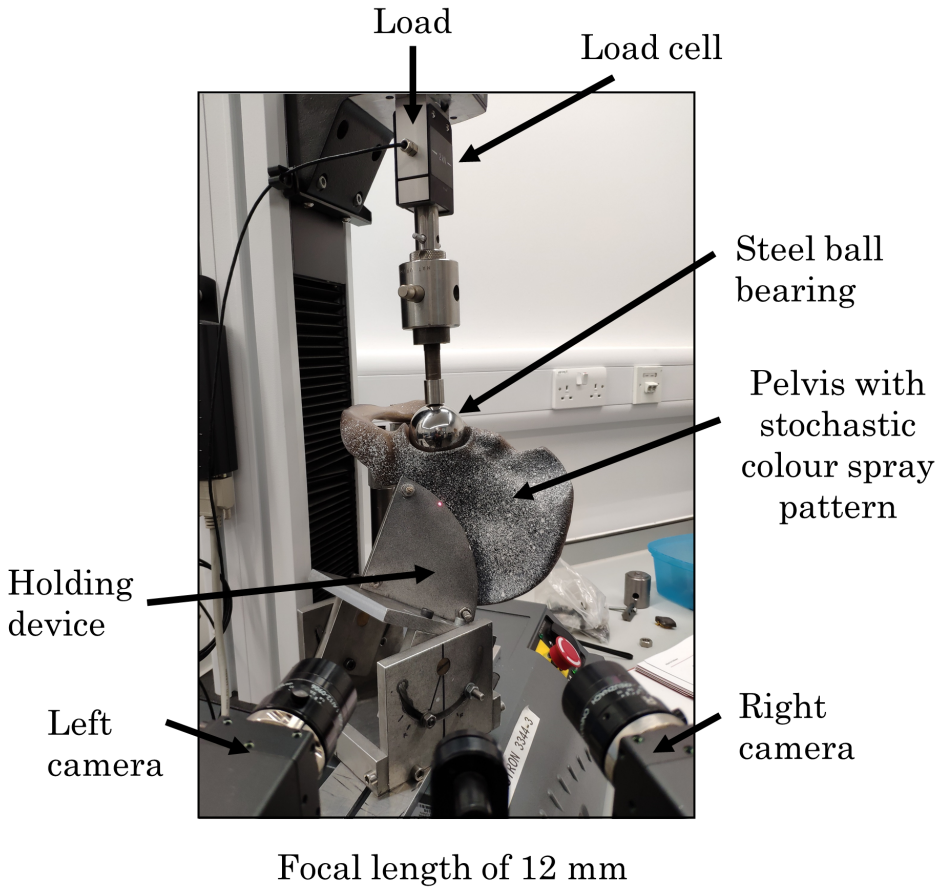

Figure 5: Experimental setup for the physical-trial experimentation. The Instron machine is shown with a 2 kN load cell the 50mm stell ball bearing fixed to the holding device and the stereoscopic camera array, a focal length of 12 mm was utilised.

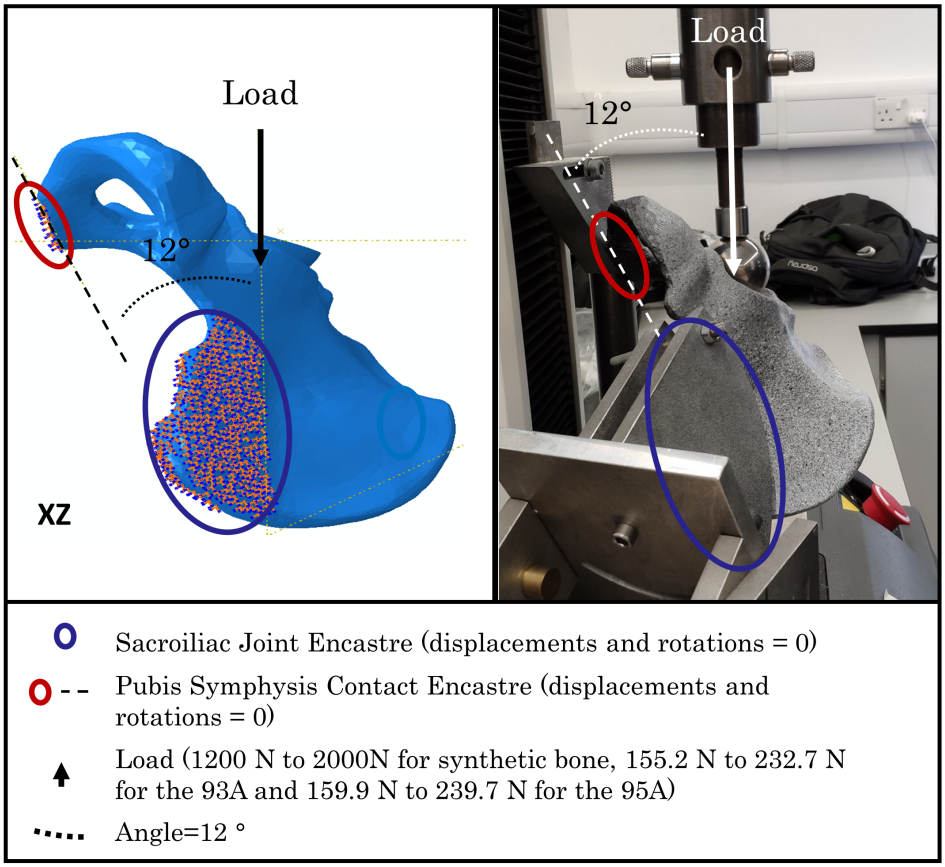

Figure 6: Comparison of the experimental setup of the physical-trial experimentation and the finite element model boundary conditions.

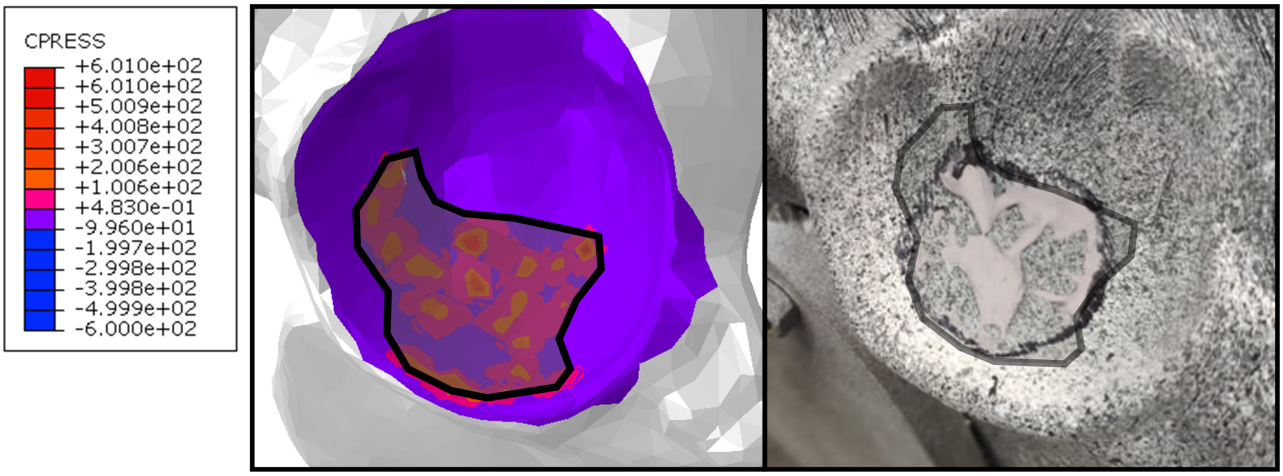

Figure 7: Comparison of contact areas. The finite element model (left) shows a similar contact pattern than the one measured in the physical experimentation (right). The quantity used for measurement in the model is the contact pressure.

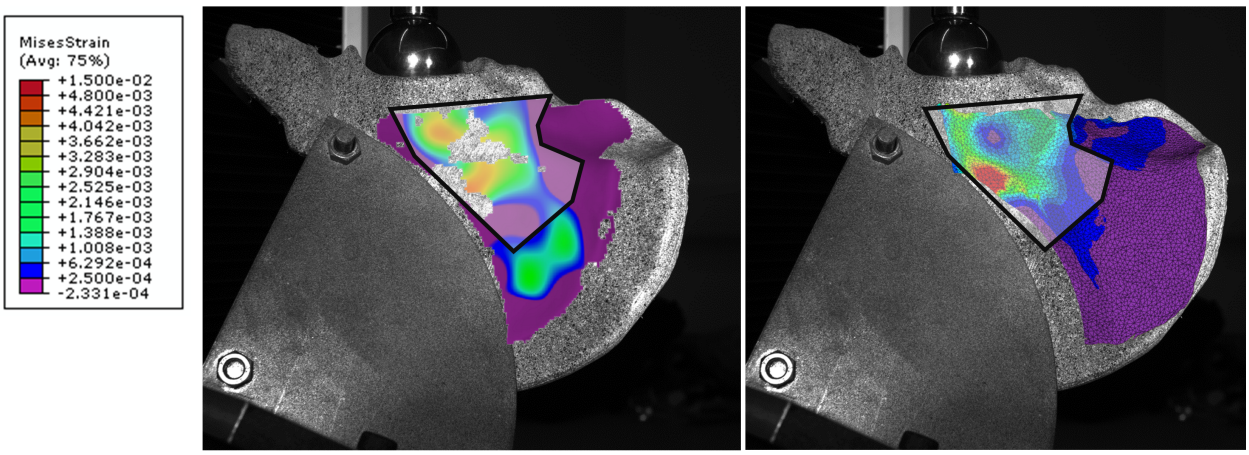

Figure 8: Visualization of the region used for measurement in the physical-trial experimentation (left) compared to the FE models measurements (right), the two images show similar von Mises strain patterns within the highlighted regions. The depth of field and measuring volume were selected to accommodate the region of interest in both scales, geometrical features outside of the region of interest have added uncertainty to the measurements and thus were not considered for comparison.

List of Tables

Material Model	$\rho(g/cc)$	E (MPa)	β	g	α_0^ρ	α_0^ν
PS: Cortical	1.64	(compressive) 16700	-	-	-	-
PS: Trabecular	0.27	155	-	-	-	-
TS1: (Cort.) PLA 0.2mm	1.25	3480	0.8 (4/5)	1.574	2.564	4.902
TS1: (Trabec.) Direct Scaling	0.206	32.3	0.8 (4/5)	1.574	2.564	4.902
TS1: (Trabec.) TPU 95A	1.2	43.83	-	-	-	-
PS1: (Trabec.) Reverse Scaling	0.492	210.3	1.25 (5/4)	0.653	0.39	0.204
TS2: (Cort.) PLA 0.4mm	1.25	3286	0.8 (4/5)	1.574	2.564	5.051
TS2: (Trabec.) Direct Scaling	0.206	30.5	0.8 (4/5)	1.574	2.564	5.051
TS2: (Trabec.) TPU 93A	1.2	30.69	-	-	-	-
PS2: (Trabecular) Reverse Scaling	0.492	155.1	1.25 (5/4)	0.635	0.39	0.198
TS3: (Cort.) PLA 0.4mm	1.25	3286	0.8 (4/5)	1.574	2.564	5.051
TS3: (Trabec.) Direct Scaling	0.206	30.5	0.8 (4/5)	1.574	2.564	5.051
TS3: (Trabec.) TPU 90A	1.2	20.84	-	-	-	-
PS3: (Trabec.) Reverse Scaling	0.492	105.9	1.25 (5/4)	0.653	0.39	0.198

Table 1: Table of the material properties and the scaling parameters of the physical space and the trial spaces for the different materials, PLA/TPU 95A (1), PLA/TPU 93A (2) and PLA/TPU 90A (3).

Microscope Analysis Images

Bone Sample	Synthetic Comp. Bone	No Overlap
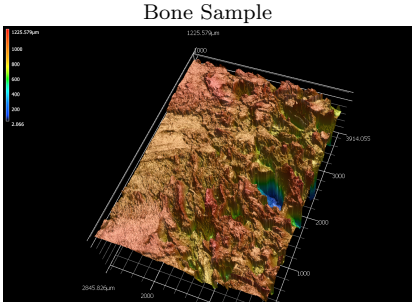	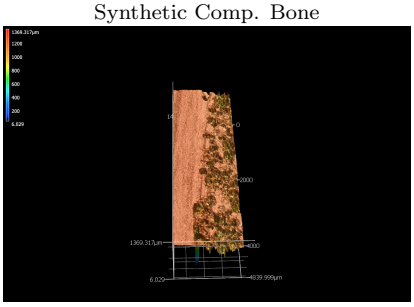	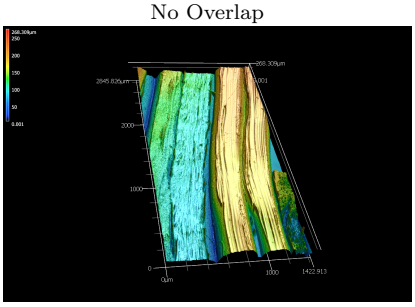
Small Overlap	**Large Overlap**	**Min. Wall Overlap**
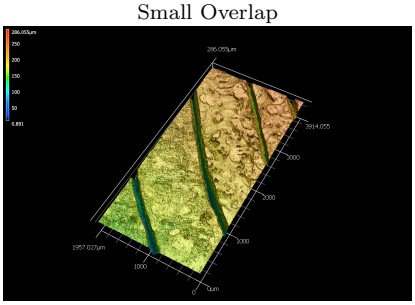	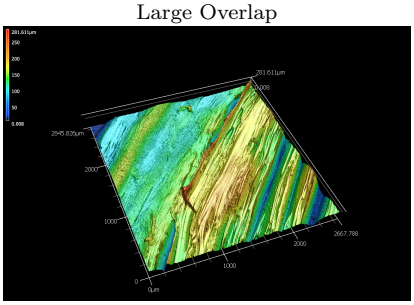	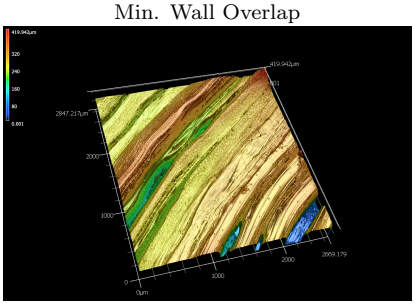

Table 2: Table with the 3D images obtained from the confocal laser scanning microscope for each of the samples analysed. The 3D printed trial space materials that resemble the physical space materials more closely are the small overlap and the minimised wall overlap samples. The bone sample was a fresh porcine femoral bone obtained from local butcher that was consequently sectioned, cleaned and finally soaked in peroxide to isolate mineral structure.

Microscope Parameters										
	Sa (μm)	Sdr	Sq (μm)	Ssk	Sku	Sp (μm)	Sv (μm)	Sdq	Spd ($1/mm^2$)	E_n
Bone	59.36	13.06	75.67	-1.09	7.72	184.52	500.38	6.22	20064.31	-
Synthetic Comp. Bone	49.23	17.89	76.13	-4.98	54.28	164.29	1214.66	7.26	41452.99	52.56
Standard Overlap	40.75	2.06	44.39	0.082	1.7	117.14	126.57	2.49	27140.8	3.92
Small overlap	17.84	6.35	23.85	-1.49	8.95	82.7	187.26	4.18	41147.76	3.29
Large overlap	23.07	4.032	29.52	-0.09	3.55	134.32	122.55	3.24	32222.56	3.6
Min. trabecular wall	28.37	4.12	42.13	-2.27	12.15	146.08	263.55	3.3	32941.44	3.35

Table 3: Table of the 3D printed exterior material properties proposed for the trial space.

Repeatability Analysis Pelvis Experiment			
	Repeatability Coeff. (%)	Mean Diff. (%)	Std. Dev. (%)
Composite Bone	0.0063	0.0009	0.0032
PLA/TPU 95A	0.0071	-0.0004	0.0036
PLA/TPU 93A	0.0061	-0.0003	0.0031
Bland Altman Statistical Analysis Pelvis Experiment			
	Mean Diff. (%)	Std. Dev. (%)	Limits of Agreement (%)
Composite Bone vs. FE Model	0.0005	0.0025	(-0.0044, 0.0055)
Composite Bone vs. PLA/TPU 95A	0.0027	0.0037	(-0.0046, 0.0100)
Composite Bone vs. PLA/TPU 93A	0.0009	0.0031	(-0.0052,0.0071)
Alternative Validation Methods			
FE model vs. PLA/TPU 95A	0.0011	0.0040	(-0.0068, 0.0091)
FE model vs. PLA/TPU 93A	-0.0004	0.0026	(-0.0056, 0.0048)

Table 4: Table with the statistical analysis of the pelvis physical-trial experimentation. The the results are presented in percentage strain and show the repeatability coefficients, mean difference (bias), standard deviation (error) and limits of agreement.

Bland Altman Plots for the Validation of FE Models

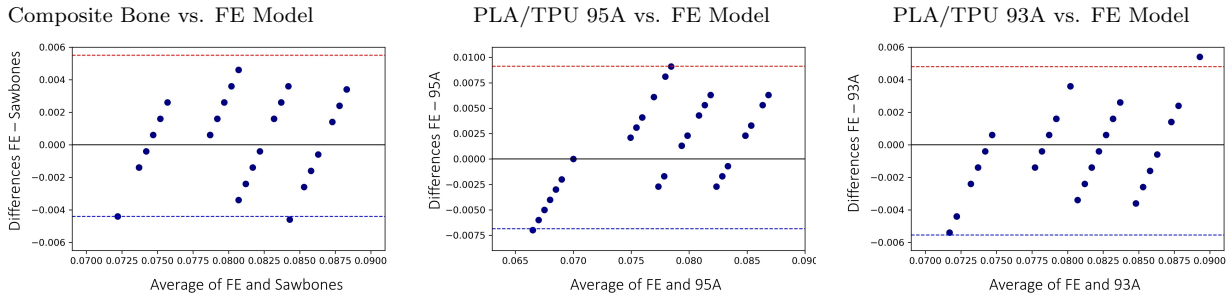

Bland Altman Plots for the Physical-Trial Experimentation

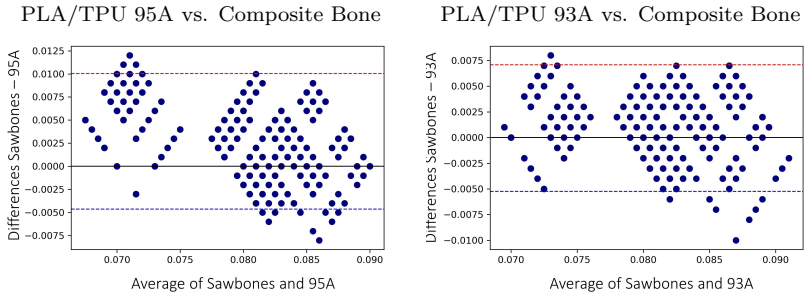

Table 5: Table with the Bland Altman plots supporting the agreement between methods of measurement, the first row showing the agreement between the finite element models and their respective experimental results and the second row showing the agreement between the phyisical and trial experimentation. The difference in strain is plotted against the mean strain, the with the 95% confidence limits (red and blue dotted lines) and the mean difference between methods (straight line).

DIC Reporting Requirements	
Camera Resolution	2448 x 2050 pixel
Focal Length	12 mm
Stereo Angle	25 degrees
Stand-Off-Distance	30 cm
Measuring Volume	200 x 160 x 160 mm^3
Image Scale	$\approx$ 14 $pixel/mm^{-1}$
Shutter Time	1.15 - 1.2 ms (varied to obtain computation start point)
Patterning Technique	Spray paint (White dull base with stochastic black pattern)
Approximate Pattern Feature Size	Close similarity with the Aramis reference spray pattern (4-7 pixels)
DIC Software Package	GOM Aramis Software v6.1
DIC algorithm	Standard subset based
Facet (subset) size	15 x 15 pixels
Facet (subset) step	13 pixels (2 pixel overlap)
Facet Shape	Square
Calibration Deviation	0.03 - 0.034 (adjusted calibration scale bar deviation $< 0.005\%$)
Calibration Object	Panel with two scale bars
Strain Formulation	Linear strain computation method (Output is chosen using Equation (22))
Computation Parameters	Computation size 3 validity quote 55%
Stage Parameters	Standard
Pre-filtering	None
Post-filtering	Average
Accuracy	0.01% or 100 micro-strains based on the configuration and parameters used
Measuring Range	0.01% up to 100%

Table 6: Table with the reporting requirements for the digital image correlation measurements following the guidelines of reference[21]. The Aramis camera configuration is 5M with a frame rate from 15 Hz up to 29 Hz.